Dependence of graphitic order of carbon nanostructures on AC and DC arc discharge methods and Ni content in thin electrode

C. R. JANG*, Gr. RUXANDA, M. STANCU, V. VOICU, D. CIUPARU**
Petroleum – Gas University of Ploieşti, Bd. Bucureşti 39, 100680, Ploieşti, Romania

In this study the graphitic order of carbon nanostructures formed on the cathode during electric arc discharges using a thin electrode with Ni were characterized by Scanning electron microscopy, X-ray diffraction and Raman spectroscopy. The results suggest that more ordered carbon nanostructures are produced when the AC arc discharge method is used for carbon nanotubes synthesis. Moreover, the more Ni contains the thin electrode, the more ordered phases are obtained, independent of the electric arc discharge method used. Further on, it can be expected that various types of carbon nanostructures besides multiwalled carbon nanotubes (MWCNTs) coexist in the plasmogenic product obtained.

(Received December 23, 2011; accepted February 20, 2012)

Keywords: Electric arc discharge, Carbon nanotubes, Raman spectroscopy, X-ray diffraction, Scanning electron microscopy

1. Introduction

Carbon nanotubes (CNTs) are the most intere- sting novel materials discovered in the last 20 years. The CNTs have started to attract attention from investigators after the primary discovery of multi- walled CNTs by Iijima [1] of NEC in 1991 during investigations of products formed by electric arc between two carbon electrodes using a high resolution transmission electron microscope (TEM). Synthesis, properties and applications of the CNTs have been studied extensively since their structure was discovered. The CNTs, as novel materials of the 21st century, can bring innovations to various industrial techniques due to their excellent mechanical, thermal conductive, electric and chemical properties. For the synthesis of graphite-like materials, including the CNTs, different techniques such as the electric arc discharge [2-6], laser ablation [7-8], chemical vapor deposition [9-12], pyrolysis of hydrocarbons [13-15], HiPCO (The High Pressure Carbon Monoxide Process) [16-17] and combined methods were used. One of the most used techniques for carbon nanostructures synthesises is the electric arc discharge, a method that uses two graphite electrodes, either with direct current (DC arc discharge) or with alternating current (AC arc discharge), and recently this technique has been used widely and efficiently [3]. For the characterization of the carbon nanostructures, X-ray diffraction (XRD), Scanning electron microscopy (SEM), TEM and Raman spectroscopy have been widely used [3, 18, 20-22]. By using the above instrumental characterization techniques, carbon nanostructures can readily be identified. As an example, Y. Ouyang and coworkers [18] provided important information on the difference of a disordered mode (DM) between singlewalled carbon nanotubes (SWCNTs) and multiwalled carbon nanotubes (MWCNTs) from Raman investigation of two species using different laser excitation energies.

We performed the CNTs synthesis by using the AC and DC arc discharge methods. During the CNTs synthesis, various types of carbonaceous materials are identified in the plasmogenic product. In this paper, SEM, XRD and Raman techniques are employed to characterize the carbon nanostructures in the plasmogenic product obtained by the AC and DC arc discharge methods using graphite rods with different diameters as electrodes. We studied the graphitic order of the carbon nanostructures in a deposit formed on a thick electrode during electric arc discharges. Further on, for all the samples, the dependence of the I_D/I_G and $I_{G'}/I_G$ ratios on the Ni content in the thin electrode is mainly discussed based on the results from the Raman investigation.

2. Experimental

2.1. Experimental setup and electrodes

The reactor designed for obtaining the plasmogenic product that contains carbon nano- structures is presented in Fig. 1. It consists of a stainless steel discharge chamber limited at both ends with flanges through which the Ar buffer gas and electrical feedings are allowed. There are two optical windows for the visualization of the arc discharge between the two electrodes in the chamber. The discharge chamber is split in two main parts: the pressure chamber and the electric arc chamber. The Ar buffer gas is released from the pressure chamber into the electric arc chamber through a separating wall (7) with 12 nozzles. The Ar gas flow is introduced in close proximity of the

electric arc zone in order to quickly remove the active nanostructure 'precursors' formed by the direct influence of the thermal radiation emitted by the electric arc. To this end, the nozzles have been oriented towards the electric arc zone to create the Ar enriched buffer gas flow in close proximity of the electrodes. For the decrease of the gas flow temperature emitted from the chamber, there is a cylindrical cooler (2) placed co-axially with the electrodes.

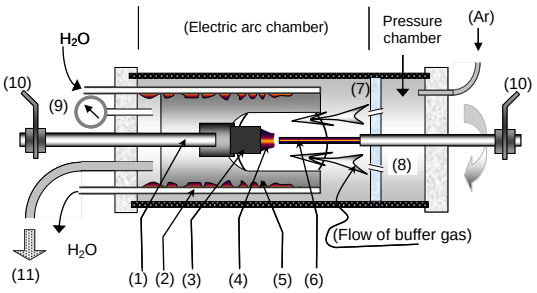

Fig. 1. Schematic diagram of the electric arc discharge setup: (1) fixed holder for the thick graphite electrode; (2) cylindrical cooler; (3) thick electrode, cathode; (4) cone-shaped deposit; (5) soot; (6) thin electrode, anode; (7) separating wall; (8) movable holder for the thin graphite electrode; (9) pressure gauge; (10) electronic contact to the electric power supply; (11) vacuum pump.

In our experiments graphite electrodes of unequal diameters with ash content below 2 ppm were used. The diameter of the thick electrode (functioning as a cathode in the DC arc discharge) is 12.05 mm and its effective length is 50 mm. The diameter of the thin electrode (the anode in the DC method) is 3.05 mm and its effective length is 105 mm. The thin electrode is loaded with nickel(Ni)-containing powder which acts as catalyst for the synthesis of the carbon nanostructures, using the following procedure. First, graphite powder is soaked in nickel acetate solution under vacuum for 20 min while the Ni component is impregnated. Then the Ni impregnated graphite powder was loaded in a thin hole of 1.4 mm diameter and 30 mm depth drilled along the longitudinal axis of the thin electrode. The pressure in the arc chamber was 0.027 MPa. The voltage and the current were kept at 20-30V and ~30 A, respectively.

2.2. Preparation of samples

The plasmogenic product is scattered all over the inner surface of the arc chamber. As it was already reported in a previous report [3], during our experiments the thin electrode is consumed, while consumption of the thick electrode has never been seen, but a cone-shaped deposit (indicated by arrow (4) in Fig. 1) is formed at its end. For the Raman and XRD investigations of the plasmogenic products obtained by the AC and the DC arc discharge methods the samples from the bottom part of the cone-shaped deposit formed at the thick electrode were selected. In order to identify the influence of the Ni content on structural order of carbon nano- structures present in the plasmogenic products obtained by the AC and DC arc discharge methods, for the DC arc discharge the Ni content was varied as 1.5 and 2.0 wt. %, while for the AC arc discharge method as 1.75 and 2.25 wt. %, respectively. Samples obtained from the thin electrodes with the Ni content of 1.5, 1.75, 2.0 and 2.25 wt.% are designated as **sample 1, sample 2 sample 3** and **sample 4**, respectively. Samples 1 and 3 were obtained by DC arc discharge while samples 2 and 4 by AC arc discharge.

2.3. Characterization of the plasmogenic products

For the investigation of the morphological, as well as structural features of the plasmogenic product obtained by the AC and DC arc discharge methods, scanning electron microscopy (SEM), XRD and Raman techniques were used. The SEM images of the samples produced by the DC and AC arc discharge methods were recorded using a Nova NanoSEM 630 instrument. The samples were dispersed and coated with Au before scanning. The XRD measurements were carried out using a Bruker D8 Advance, X-ray diffractometer with Cu Kα radiation (λ_{Cu} = 0.1541 nm), operating at a voltage of 40 kV and a current of 40 mA, at room temperature. The XRD patterns were recorded in 2θ range from 10.0° to 60°, with a scanning rate of 0.1 deg·min^{-1}. The Raman spectra of the samples were recorded on a Jasco Laser Raman Spectrophotometer NRS-3000 Series with laser excitation energies of 532 nm (E_L=2.33 eV) and 1 cm^{-1} resolution.

3. Results and discussion

3.1. SEM

The SEM technique is used to characterize the size and morphology of the plasmogenic product obtained. The SEM images of samples 1 and 3 obtained using the DC arc discharge, are shown in Fig. 2(a) and 2(c), and the ones of samples 2 and 4 obtained by the AC arc discharge method are shown in Fig. 2(b) and 2(d), respectively. For the studied samples, the SEM images show that carbon nanostructures obtained consist mainly of two components, in which the tubular component is quantitatively smaller than the granular component (approximately 25 nm in size). It is presumed that the granular component intrinsically contains an amorphous part and the tubular component consists of MWCNTs type nanostructures. In the images, it can be clearly seen that the tubular components with outer diameter between 5 and 23 nm are present in the plasmogenic products and these components are apparently developed from granular conglomerates, and a tubular component is also developed from an inner side of one with larger diameter, like a telescopic tube (See Fig. 2 (a)).

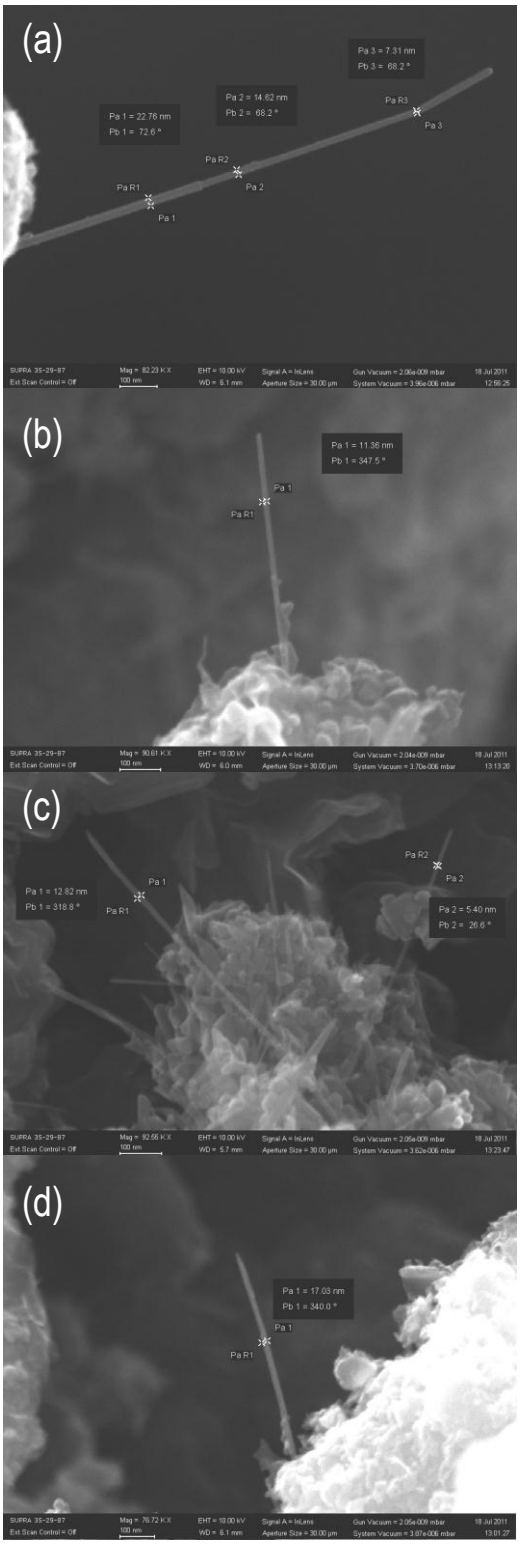

Fig. 2. SEM images of the carbon nanostructures obtained by the electric arc discharge methods: (a) Sample 1, (b) Sample 2, (c) Sample 3, (d) Sample 4.

3.2. X ray diffraction

In Fig. 3 are shown the XRD patterns of samples selected from the deposits resulting from AC and DC arc discharge experiments. An intense peak at 2θ of 26.1~26.2^o, representing the (002) graphitic basal plane reflection in carbon nanostructures, can be clearly seen for all samples obtained by the AC and DC arc discharge methods. The interlayer distances of (002) planes calculated using the Maire and Mering formula [19] for all the samples are in region of 0.3415~0.3402 nm. This value is slightly larger than that of normal graphite (d_{002}=0.3355 nm) [20]. The peak intensities at 2θ 26.1~26.2^o of samples 1 and 3 obtained by the DC method are slightly lower than those of samples 2 and 4 by the AC method. The difference between the four peak intensities suggests that there is a difference in their crystallographic structures and in the degree of crystallization of the carbon nanostructures present in the plasmogenic products obtained by the two methods. On the other hand, relatively weak peaks are also observed near 2θ of 42.9^o and 54^o, corresponding to (100) and (004) planes of the graphite structure [20-21]. However, the XRD patterns of all the samples showed the diffusing peaks of (100) and (101) planes of graphite, indicating the presence of carbonaceous materials with turbostratic structure [22] in the plasmogenic products. It is well known that XRD pattern of amorphous carbon is characterized by the presence of only two peaks corresponding to the (002) and (100) planes. Our findings suggest that granular particles, which can be seen in the SEM images, have the turbostratic structure and include amorphous carbon. Fig. 4 shows the atomic structure of a turbostratic graphite. This figure indicate that, unlike the normal hexagonal structure of graphite (Fig. 4(a)), the unit cell structure is deformed (Fig. 4(b)) due to a rotation of the graphene sheet B in the AB stacked graphene layers. Thus, it should include a small number of carbon atoms in the (100) and (101) planes and the number of scattering centers should be reduced in comparison with that in the unit cell of the graphite (hexagonal, rhombohedral, orthorhombic). Therefore, the peaks of the (100) and (101) lattice planes of graphite-like materials with the turbostratic structure are widened and their intensities are weakened. These results are not in agreement with previous research result of P. Trucano and R. Chen [20], which show that $I_{(101)} \cong 4I_{(100)}$. For the diffraction of the (100) plane, the height and sharpness of the peaks of samples 1 and 3 are also slightly lower than the ones of samples 2 and 4. This indicates that the degree of crystallization of the plasmogenic product obtained by the AC arc discharge is higher than that produced by the DC method and, therefore, the XRD analysis suggests that the AC arc discharge products have more ordered carbon nanostructures than the ones obtained by the DC method.

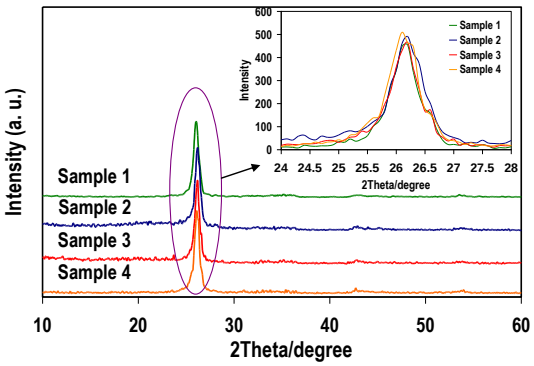

Fig. 3. XRD patterns of the CNTs obtained by the AC and the DC arc discharge methods. Inset shows the diffraction peaks at 2θ of 26.1~26.2°.

Moreover, from the XRD patterns of the (002) and (100) planes we found that the peak intensities increase with the Ni content used in the thin electrode, independently of the electric arc discharge method used, suggesting that the carbon nanostructures improve in graphitic order, as the Ni content in the thin electrode increases.

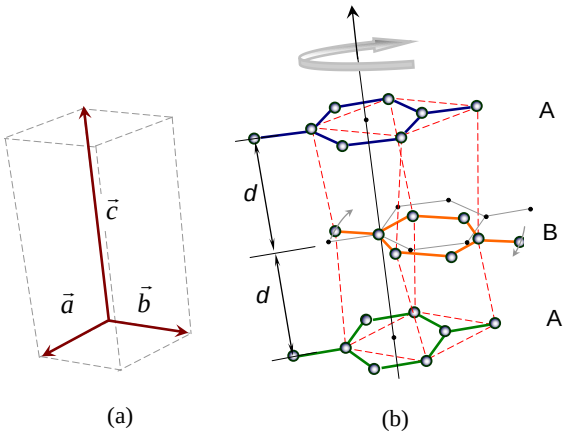

Fig. 4. Schematic illustration of atomic structure of turbostratic carbon: (a) hexagonal unit cell of graphite, (b) unit cell structure deformed as a result of rotating of graphene sheet B for turbostratic carbon.

3.3. Raman spectroscopy

Generally, the carbon nanostructures features are represented by the graphite band (G band) attributed to the tangential stretching vibrations of graphitic structures with sp^2 type of bonding and D band associated with disordered or defective graphenic structures. Fig. 5 shows the Raman spectra of carbon nanostructures in the plasmogenic product obtained by using laser excitation at 532 nm. In the first order Raman spectra (Fig. 5(a)) of all selected samples, two main peaks, the D band peak at around 1353 cm^{-1} and the G band peak at around 1584 cm^{-1} are identified, which are evidence for the presence of both defective and ordered carbonaceous materials. It is observed that the difference between the Raman spectra of all samples is the increase in the G band intensity with increasing of the Ni content in the thin electrode. The increase of the G band intensity suggests better graphitic structure of the product obtained using the AC arc discharge method than that resulting from the DC method.

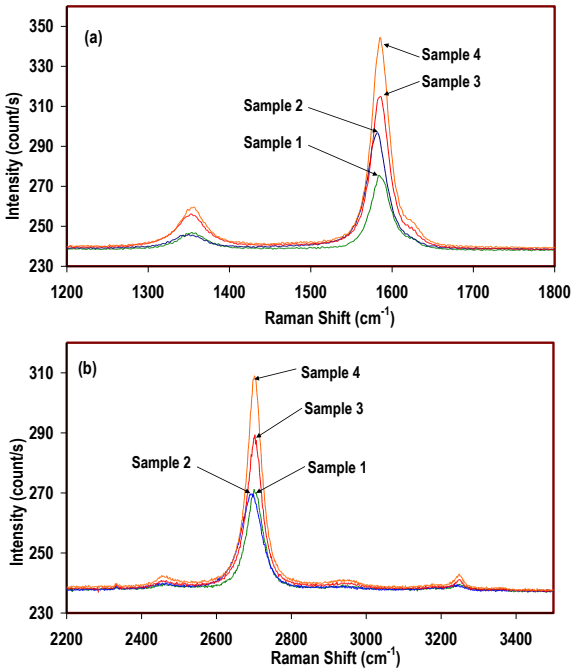

Fig. 5. Raman spectra of the samples obtained by the AC and the DC arc discharge methods: (a) The first order Raman spectra, (b) The second order Raman spectra.

The disorder-induced D band is also found to blue-shift with the increase of the Ni content. On the other hand, the second order Raman spectra in the 2200-3500 cm^{-1} region (Fig. 5(b)) also show four peaks, a shoulder peak at around 2455 cm^{-1}, the G' band (first overtone of the D mode) with a prominently strong intensity at around 2702 cm^{-1}, the D+G mode at around 2938 cm^{-1} and the 2D' band (G band overtone) at around 3245 cm^{-1}. These peaks are the second order Raman features of all graphite-like materials including MWCNTs [22-23]. Although the G' band corresponds to a two-phonon process and its orgin is independent of the structural disorder in the carbonaceous materials, Fig. 5(b) shows that the intensity and the position of this band are sensitive to the Ni content of the samples.

Table 1 describes the positions and intensities of the D, G and G' bands. One can see that the shift in the intensity and position of the G' band with the Ni content is similar to that of the D band. The Raman intensity of the G band increases with the Ni content in the thin electrode. In case of the D and G' bands the increase of the Ni content from 1.5 to 1.75 wt.% leads to a slight decrease of the intensities, while from 1.75 to 2.25 wt.% there is an increase. Moreover, the shift of the positions of the D (by 7 cm^{-1}) and G' (by 12 cm^{-1}) bands is observed with the increase of

the Ni content for samples obtained by the AC arc discharge, while a slight shift of the D and G' bands for the ones obtained by the DC method is identified. A blue-shifting of the D band for the samples obtained by using AC arc discharge may suggest that new types of disorders, including surface defects of the MWCNTs, appear. The G' band is not related to the structural defects of the graphite-like materials and it can be used to determine the number of graphene layers [22]. We found that the G' band feature of all samples has a single peak only at the corresponding position around 2702 cm^{-1}. Such feature of the G' band in Raman spectra indicates that graphite-like materials with turbostratic structure have been produced during the electric arc discharge.

Table 1. Position and intensity of the main peaks in Raman spectra of the investigated samples with Ni content.

	Peak	Ni content in the thin electrode, wt. %			
		1.5 (DC)	1.75 (AC)	2.0 (DC)	2.25 (AC)
Raman shift, cm^{-1}	D	1354	1350	1353	1357
	G	1584	1582	1586	1585
	G'	2701	2690	2703	2702
Intensity	D	246.9	245.9	256.2	259.6
	G	275.5	296.8	315.0	344.4
	G'	271.2	269.7	289.2	309.0

Fig. 6 shows the fitted curves plots of the I_D/I_G and $I_{G'}/I_G$ ratios, which are calculated from the intensity values in Table 1, depending on the Ni content in the thin electrode. Two plots are depicted using linear fitting. The variations presented in Fig. 6 confirm the dependence of the I_D/I_G and $I_{G'}/I_G$ ratios as a function of the Ni content in the thin electrode. One can clearly see that the increase in the Ni content in the thin electrode results in the decrease of the I_D/I_G and $I_{G'}/I_G$ ratios. It is known that the increase in the ratio between the intensities of the D and G bands, I_D/I_G value, corresponds to the presence of more structural defects in the carbonaceous materials [3, 18, 22]. The decrease of the I_D/I_G ratio reveals the increase of the graphitic order of the carbon nanostructures with the increase of the Ni content, meaning that more ordered nanostructures are obtained, as the thin electrode contains larger amounts of Ni, which acts as catalyst for the growth of the carbon nanostructures, including MWCNTs, independent of the electric arc discharge methods used. Also, it shows that the defect concentration in the carbon nanostructures obtained using the AC arc discharge method is slightly lower than the one obtained by the DC method, meaning that relatively more ordered phases exist in the materials obtained by the AC arc discharge method. This is in good agreement with the XRD results discussed above. In addition to these results, we also found that the $I_{G'}/I_G$ ratio decreases when the Ni content increases. Although the reason for this is not clear due to the coexistence of carbonaceous materials with different structures in the carbon nanostructures obtained, it is worth further investigation.

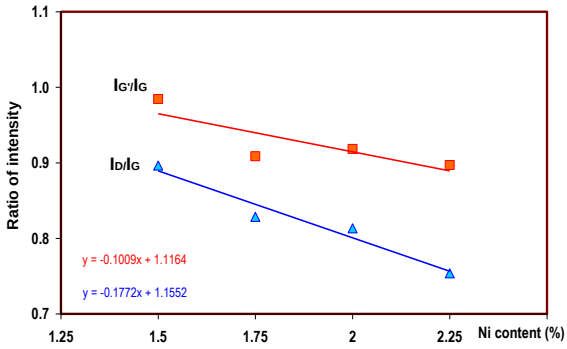

Fig. 6. Dependence of the I_D/I_G and $I_{G'}/I_G$ ratios for all samples obtained by the AC and the DC methods on Ni content in the thin electrode.

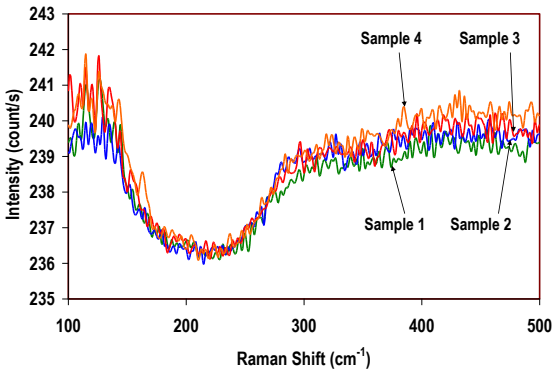

Fig. 7. Raman spectra in region of 100-500 cm^{-1} for all samples investigated.

On the other hand, we observed the Raman spectra in the 100-500 cm^{-1} region in order to determine which types of CNTs are produced during the electric arc discharge. The low frequency region of the spectrum, where the Radial Breathing Mode (RBM) vibrations appear, in the 100-400 cm^{-1} region, is a second part characteristic of SWCNTs. Fig. 7 represents the Raman spectra in the 100-500 cm^{-1} region for all samples investigated. When the laser excitation of 514 nm is used, in case of SWCNTs, peaks with strong intensities appear in this region, but in the case of MWCNTs peaks do not appear [24]. In Fig. 7 one can see that the bands characteristic to RBM did not appear in this region of the Raman spectra, independent of the electric arc discharge methods or the Ni content in the thin electrode. This fact suggests that all samples contain only MWCNTS and not SWCNTs. This analysis result is consistent with the above SEM observations.

4. Conclusions

The samples discussed in this paper were synthesized using the AC and DC arc discharge methods, using the same conditions of Ar buffer gas pressure and discharge current intensity. From SEM, XRD and Raman investigations of the samples, selected from the bottom part of the cone-shaped cathode deposits formed at the end of the thick electrode during the arc discharge, we observed that different types of carbon nanostructures exist in the plasmogenic product. As observed from SEM images, in the plasmogenic product coexist both granular and tubular structures. The latter have multilayer structure and graphite characteristics depending on the diameters of the tubular structures. This observation is also sustained by the XRD investigation showing a slight shift of the specific graphitic peak. The results of XRD and Raman investigations prove the presence of the graphitic carbon in the nanostructured materials. They show that the ordered phases are relatively more abundant in carbon nanostructures obtained by the AC arc discharge method. Moreover, we conclude that the more Ni contains the thin electrode, the more ordered nanostructures are obtained, independent of the electric arc discharge method used. In addition, the XRD and Raman investigations suggest that the granular particles have the turbostratic structure and include amorphous carbon.

Acknowledgements

This research has been supported by the doctoral program of Romanian Ministry of National Education (No. 37526/CMJ/22.11.2007, No. 38194/CMJ/ 12.05.2011).

References

[1] S. Iijima, Nature, **354**, 56 (1991).
[2] M. Endo, T. Hayashi, Y. A. Kim, H. Muramatsu, Jap. J. App. Phys., **45**, (6A), 4883 (2006).
[3] Gr. Ruxanda, M. Stancu, S. Vizireanu, G. Dinescu, D. Ciuparu, J. Optoelectron. Adv. Mater, **10**(8), 2047 (2008).
[4] S. Cui, P. Scharff, C. Siegmund, D. Schneider, K. Risch, S. Klötzer, L. Spiess, H. Romanus, J. Schawohl, Carbon, **42**(5-6), 931 (2004).
[5] Y. Y. Tsai, J. S. Su, C. Y. Su, Inter. J. Mach. Tools Man., **48**(15), 1653 (2008).
[6] A. Mansour, M. Razafinimanana, M. Monthioux, M. Pacheco, A. Gleizes, Carbon, **45**(8), 1651 (2007).
[7] T. Ikegami, F. Nakanishi, M. Uchiyama, K. Ebihara, Thin Solid Films, **457**(1), 7 (2004).
[8] H. Dai, A. G. Rinzler, P. Nikolaev, A. Thess, D. T. Colbert, R. E. Smalley, Chem. Phys. Lett., **260**(3-4), 471 (1996).
[9] Ç. Öncel, Y. Yürüm, Fullerenes, Nanotubes and Carbon Nanostructures, **14**, 17 (2006).
[10] Y. An, X. Yuan, S. Cheng, X. Gen, Rare Metals, **25**(6), 73 (2006).
[11] Q. H. Wang, A. A. Seltlur, J. M. Lauerhaas, J. Y. Dai, E. W. Seelig, R. P. H. Chang, Appl. Phys. Lett., **72**(22), 2912 (1998).
[12] X. Xu, G. R. Brandes, Appl. Phys. Lett., **74**(17), 2549 (1999).
[13] Al. Darabont, P. Nemes-Incze, J. Optoelectron. Adv. Mater., **7**(2), 631 (2005).
[14] K. Suenaga, M. P. Johansson, N. Hellgren, Chem. Phys. Lett., **300**(5-6), 695 (1999).
[15] W. K. Hsu, J. P. Hare, M. Terrones, H. W. Kroto, D. R. M. Walton, P. J. F. Harris, Nature, **377**(6551), 687 (1995).
[16] Y. Mackeyev, S. Bachilo, K. B. Hartman, L. J. Wilson, Carbon, **45**(5), 1013 (2007).
[17] L. G. Bulusheva, A. V. Okotrub, U. Dettlaff -Weglikowska, S. Roth, M. I. Heggie, Carbon, **42**(5-6), 1095 (2004).
[18] Y. Ouyang, L. M. Cong, L. Chen, Q. X. Liu, Y. Fang, Physica E: Low-dimensional Systems and Nanostructures, **40**(7), 2386 (2008).
[19] M. A. Ermakova, D. Y. Ermakov, A. L. Chuvilin, G. G. Kuvshinov, J. Catal., **201**, 183 (2001).
[20] P. Trucano, R. Chen, Nature, **258**, 136 (1975).
[21] A. Dandekar, R. T. K. Baker, M. A. Vannice, Carbon, **36**(12), 1821 (1998).
[22] M. A. Pimenta, G. Dresselhaus, M. S. Dressel-haus, L. G. Cancado, A. Jorio, R. Saito, Phys. Chem. Chem. Phys., **9**, 1276 (2007).
[23] E. F. Autunes, A. O. Lobo, E. J. Corat, V. J. Trava-Airoldi, A. A. Martin, C. Verissimo, Carbon, **44**(11), 2202 (2006).
[24] E. Flahaut, Ch. Laurent, A. Peigney, Carbon, **43**(2), 375 (2005).

*Corresponding author: chol.hciu@yahoo.com,
**dciuparu@upg-ploiesti.ro